Chiral Emissive Lanthanide Complexes from Enantiopure [6]Helicene-bis(pyrazolyl)-pyridine Ligands

Alexandre Abherve, Maurizio Mastropasqua Talamo, Nicolas Vanthuyne, Francesco Zinna, Lorenzo Di Bari, Maxime Grasser, Boris Le Guennic, N. Avarvari

10.1002/ejic.202200010

Chiral Emissive Lanthanide Complexes from Enantiopure [6]Helicene-bis(pyrazolyl)-pyridine Ligands

Alexandre Abhervé,*[a] Maurizio Mastropasqua Talamo,[a] Nicolas Vanthuyne,[b] Francesco Zinna,[c] Lorenzo Di Bari,[c] Maxime Grasser,[d] Boris Le Guennic*[d] and Narcis Avarvari*[a]

[a] *Dr. A. Abhervé, Dr. M. Mastropasqua Talamo, Dr. N. Avarvari, Univ Angers, CNRS, MOLTECH-Anjou, SFR MATRIX, F-49000 Angers, France. E-mail: alexandre.abherve@univ-angers.fr; narcis.avarvari@univ-angers.fr*

[b] *Dr. N. Vanthuyne, Aix Marseille Université, CNRS, Centrale Marseille, iSm2, Marseille, France*

[c] *Dr. F. Zinna, Prof. L. Di Bari, Dipartimento di Chimica e Chimica Industriale, Università di Pisa, via G. Moruzzi 13, 56124, Pisa, Italy*

[d] *M. Grasser, Dr. B. Le Guennic, Univ Rennes, CNRS, ISCR (Institut des Sciences Chimiques de Rennes) – UMR 6226, F-35000 Rennes, France. E-mail: boris.leguennic@univ-rennes1.fr*

Abstract: Enantiopure helicene-based bis(pyrazol-1-yl)pyridine (bpp-[6]helicene), with the helicene unit in position 4 of the pyridine ring, have been prepared and structurally characterized. Their chiroptical properties have been studied experimentally, and both absorption and circular dichroism (CD) spectra have been reproduced theoretically by time-dependent density functional theory (TDDFT). Remarkably, in spite of the remote localization of the helicene with respect to the coordination pocket of the bpp motif, chiral Eu(III) complexes based on these ligands show, however, circularly polarized luminescence in the visible region, sustained by TDDFT and CASSCF calculations, which also emphasize the possible antenna effect of the bpp ligand.

Introduction

Helicenes constitute valuable building blocks provided with intrinsic helical chirality, which attracted much attention in recent years in the field of chiral materials.[1] Their exceptional chiroptical properties such as high optical rotation, intense electronic circular dichroism (ECD) and circularly polarized luminescence (CPL),[2] especially for heterohelicenes,[3] are related to their peculiar helical π-conjugated skeleton. Attachment of coordinating groups on the helicene platform results in helicene based ligands and corresponding transition metal complexes. The latter started to be investigated especially since 2008,[4] in order to obtain innovative chiral complexes which combine the properties of the helicene unit with those of the metal centre,[5] resulting, for example, in original chiroptical,[6,7] CPL,[8,9] or magnetic properties.[10,11] Moreover, very recently, the use of azahelicene appended pyridine ligands[8] allowed the preparation of an ytterbium(III) complex showing strong magneto-chiral dichroism.[12] In the frame of our own interest in functional helicenes,[13,14] and their transition metal complexes,[9,15] we have recently reported the series of 2,6-bis(pyrazol-1-yl)pyridine (1-bpp) ligands substituted by racemic [4]-, [5]- and [6]helicene units in the 4-position of the pyridine ring, together with the photophysical properties of their luminescent Re(I) and Ru(II) complexes.[16] While a large variety of functionalized 1-bpp and corresponding transition metal complexes have been reported,[17,18] chiral derivatives have received little attention so far,[19,20] especially driven by catalytic applications,[21,22] but not for emission or chiroptical properties. Although several examples of photoemissive lanthanide complexes based on the 1-bpp ligand have been reported,[23–26] no example of such chiral complexes has been described so far, to the best of our knowledge. Indeed, chiral ligands employed so far in CPL active lanthanide complexes span from macrocycles,[27–32] camphor or other chiral ketone derivatives,[33–37] dipicolinate-based architectures,[38–40] pyridine oxazoline compounds[41,42] and bipyridine-based cryptates.[43,44] Although the position of the chiral helicene unit

10.1002/ejic.202200010

in our ligands is remote from the coordination pocket of the bpp, we aimed however in this study at investigating the ability of both (*M*) and (*P*) enantiomers of 2,6-bis(pyrazol-1-yl)pyridine-4-[6]helicene, hereafter called **6*M*** and **6*P***, to polarize the luminescence of tris(2-thenoyltrifluoroacetonate)lanthanide(III) complexes (Scheme 1). Actually, in a few instances, it has been observed that it is not necessary to have a chiral coordination polyhedron in order to observe sizeable CPL activity, especially when a dynamic coupling between f-f and induced ligand-centered transitions is at play.[45,46] We report herein the synthesis, structural characterization and chiroptical properties of **6*M*** and **6*P***, together with the chiroptical and CPL properties of their red-emissive europium(III) and NIR-emissive ytterbium(III) complexes, supported by time-dependent density functional theory (TD-DFT) and complete active space self-consistent field (CASSCF) calculations.

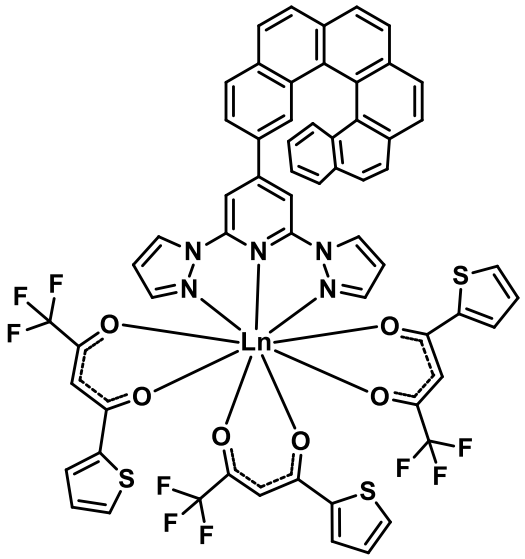

Ln = Eu, Yb

Scheme 1. Structure of the bpp[6]helicene-based lanthanide(III) complexes.

Results and discussion

Synthesis, chiroptical properties and structures of 6*M* and 6*P*

The racemic 1-bpp[6]helicene ligand was prepared according to our recent report.[16] The precursor dichloropyridine-[6]helicene was obtained by a Suzuki coupling between 2-bromo[6]helicene and 2,6-dichloropyridine-4-boronic acid pinacol ester. After reaction with sodium pyrazolate, 1-bpp[6]helicene was obtained as a racemic mixture and characterized by ^{1}H and ^{13}C NMR and mass spectrometry (Figures S1-S3). The *M* and *P* enantiomers were separated by semi-preparative chiral HPLC on Chiralpak IE (250 x 10 mm, Figures S4-S6). Optical rotations and circular dichroism (CD) spectra were determined for both enantiomers (Figures 1 and S7). It was found that the *M* enantiomer was levorotatory, with optical rotation values of -2400, -2550, -3300 and -10500 deg·mL·g^{-1}·dm^{-1} at 589 nm, 578 nm, 546 nm and 436 nm, respectively. Opposite values were measured for the dextrorotatory *P* enantiomer. Interestingly, drop-casted thin films of **6*M*** and **6*P*** show a more intense band at 380 nm and a much weaker band at higher energy compared to solution measurements, together with a broadening of the absorption band, very likely a consequence of intermolecular interactions between the helicene units and/or conformational restrictions in the solid state (Figure 1).

10.1002/ejic.202200010

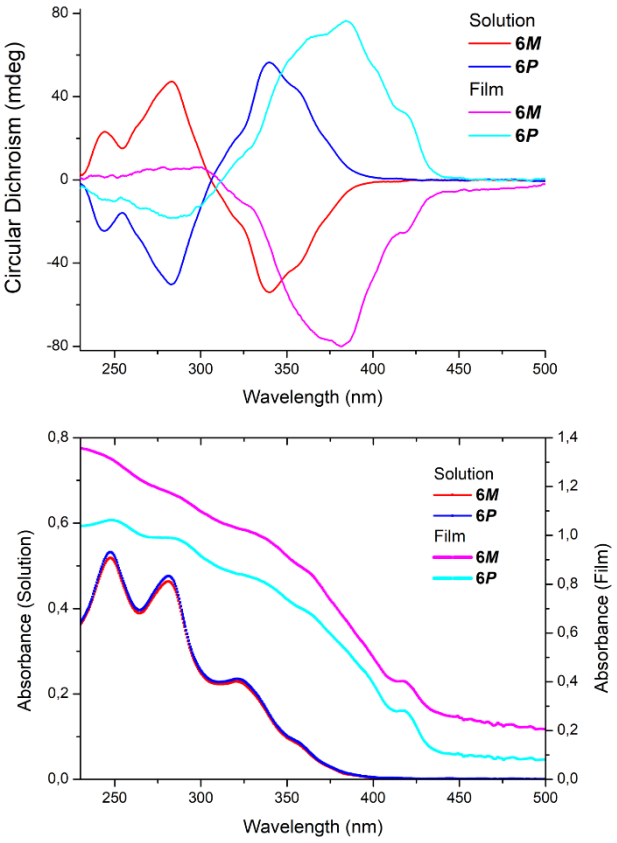

Figure 1. CD (top) and UV-Vis (bottom) spectra of ***6M*** and ***6P*** in 10^{-5} M dichloromethane solution and in thin film.

The absolute configuration of the ligands was further confirmed by single-crystal X-ray diffraction measurements (Figure 2, Table S1). Both enantiomers ***6M*** and ***6P*** crystallized in the non-centrosymmetric monoclinic space group $P2_1$ with two independent molecules in the asymmetric unit (Figure S8).

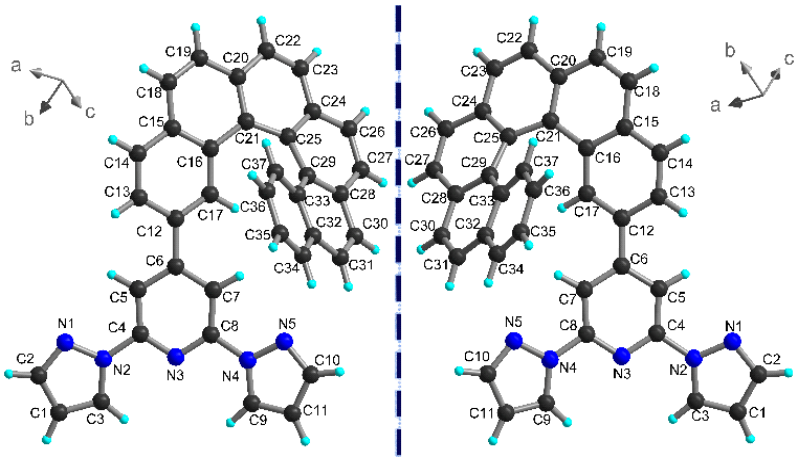

Figure 2. Crystal structure of ***6M*** (left) and ***6P*** (right) with atom label. Color code: C (black), H (cyan), N (blue).

The inherent helical chirality of the molecule is characterized by the helical curvature, that is the dihedral angle between first and last aromatic rings of helicene, with values of 46.14(9) – 48.82(11)° and 48.86(9) – 50.56(8)° in ***6M*** and ***6P***, respectively (Figures S9 and S10). The biphenyl type connection between pyridine and first benzene ring of the helicene scaffold leads to torsion angles of 28.11(8) – 29.39(8)° in ***6M*** and 28.22(8) – 28.95(8)° in ***6P***. Selected bond distances and angles are summarized in Table S2.

Synthesis and chiroptical properties of the complexes

Next, with the enantiopure **6*M*** and **6*P*** in our hands, we synthesized both red-emissive [Eu(tta)$_3$(**6*M***)] and [Eu(tta)$_3$(**6*P***)] and NIR-emissive [Yb(tta)$_3$(**6*M***)] and [Yb(tta)$_3$(**6*P***)] (tta$^-$ = 2-thenoyltrifluoroacetonate, see ESI for characterization of the complexes, Figures S11-14). Mass spectrometry measurements confirmed the coordination of the 1-bpp[6]helicene ligands to the lanthanide centers. While similar UV-Vis spectra were observed, mirror-image CD spectra were obtained for both Yb and Eu **6*M*** and **6*P***-based complexes in 10^{-5} M CH_2Cl_2 solution (Figure 3).

The emission properties in solution, at RT, of **6*M*** and **6*P*** ligands and of the corresponding Eu and Yb complexes have been investigated (Figures S15-S16). While both complexes present a small residual fluorescence of the coordinated 1-bpp[6]helicene ligand, suggesting an incomplete ligand-to-metal energy transfer, they also show typical bands for the transitions associated to the emission of the lanthanide.

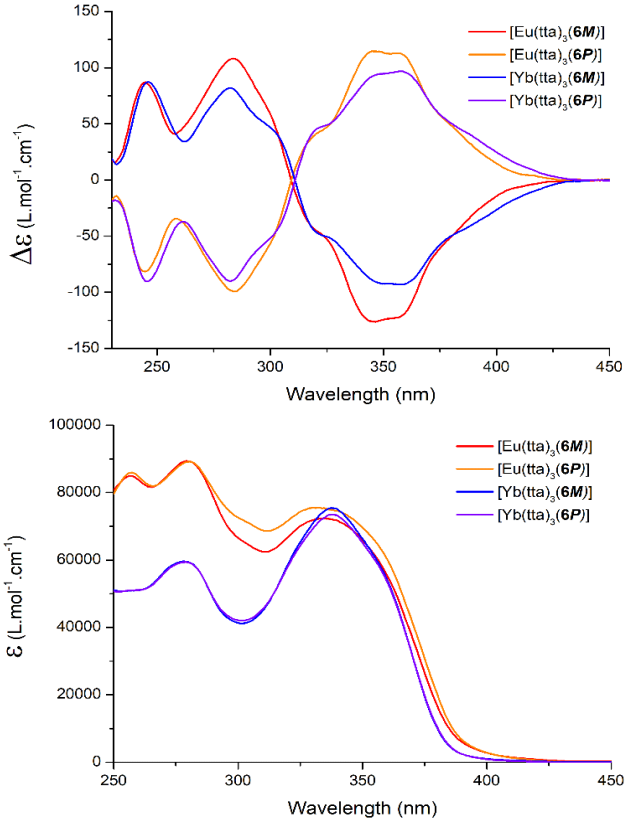

Figure 3. CD (top) and UV-Vis (bottom) spectra of the complexes in 10^{-5} M dichloromethane solution.

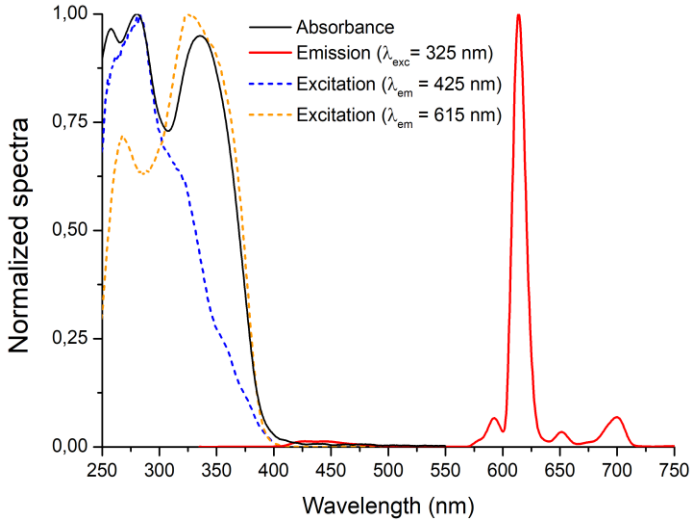

Figure 4. Normalized absorption, emission and excitation spectra of [Eu(tta)$_3$(**6*M***)].

The total quantum yield of luminescence in [Eu(tta)$_3$(**6*M***)] is 32%, which is slightly higher than in the complex precursor [Eu(tta)$_3$(H$_2$O)$_2$] (Φ = 23%). Two excitation spectra for [Eu(tta)$_3$(**6*M***)] were recorded at λ_{em} = 425 nm and λ_{em} = 615 nm, corresponding to the maximum emission of **6*M*** and Eu(III) respectively (Figure 4). While the former matches the absorption spectrum of the ligand **6*M***, the latter suggests a predominant absorption of the tta$^-$ anion for the luminescence of the lanthanide ion, yet the participation of **6*M*** is supported by comparison with the excitation spectrum of the complex precursor [Eu(tta)$_3$(H$_2$O)$_2$] (Figure S17) as well as theoretical calculations (*vide infra*).

Subsequently, CPL measurements have been performed on CH_2Cl_2 solutions of both Eu and Yb complexes. Remarkably, in spite of the weak conjugation between helicene and bpp moieties and the remote localization of the chiral unit with respect to the coordinated Eu(III) ion, [Eu(tta)$_3$(**6*M***)] and [Eu(tta)$_3$(**6*P***)] display weak but measurable CPL signals. In particular, mirror image signals associated to the $^7F_1 \longleftarrow {}^5D_0$ transition were detected (Figure 5). Such signals display a dissymmetry factor g_{lum} of $\pm 3 \cdot 10^{-3}$ (positive for the *P* enantiomer, negative for the *M* enantiomer).

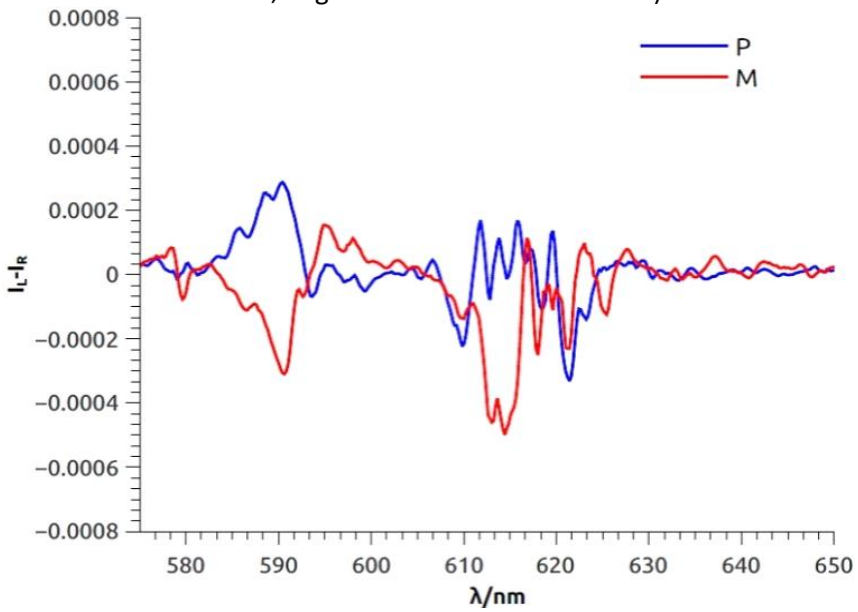

Figure 5. CPL spectra of [Eu(tta)$_3$(**6*M***)] and [Eu(tta)$_3$(**6*P***)] in 10^{-5} M dichloromethane solution.

On the other hand, the signals associated to the $^7F_2 \longleftarrow {}^5D_0$ transition appear very noisy due to a much lower dissymmetry factor (estimated ~ 10^{-4}). These relatively low values with respect to other Eu(III)

CPL active complexes with pyridine-bis(oxazoline) ligands strongly support the determinant role of the position of the chiral elements with respect to the metal center. In particular, these results would highlight that in this type of heteroleptic complexes, the main role in CPL activity is played by the stereo-ordered arrangement of the diketonates around the lanthanide, provided such order is efficiently imparted by properly placed chirality elements.[47,48] Although [Yb(tta)$_3$(**6*M***)] and [Yb(tta)$_3$(**6*P***)] display easily measurable NIR luminescence with maximum around 975 nm (Figure S18), in this case, it was not possible to unambiguously measure mirror image CPL signals, possibly due to the weakly polarized emission ($g_{lum} < 10^{-3}$, Figure S18). However, NIR-CPL active Yb(III) complexes are still very rare in the literature,[49-53] therefore intensive endeavor in this direction is required in order to understand the role of the ligand chirality on the polarized emission of the lanthanide. These results show that the **6*M***/**6*P*** scaffold may be at the limit of polarizability induction for such emissive lanthanide complexes.

Theoretical calculations

Further, the **6*M*** ligand and the corresponding Eu(III) and Yb(III) complexes have been studied theoretically in order to support the experimental findings. Density functional theory (DFT) was applied to obtain structural geometries and to gain insight into the optical and chiroptical properties of the ligands whereas multi-configurational wave function approaches were employed to simulate chiroptical properties of the lanthanide complexes.

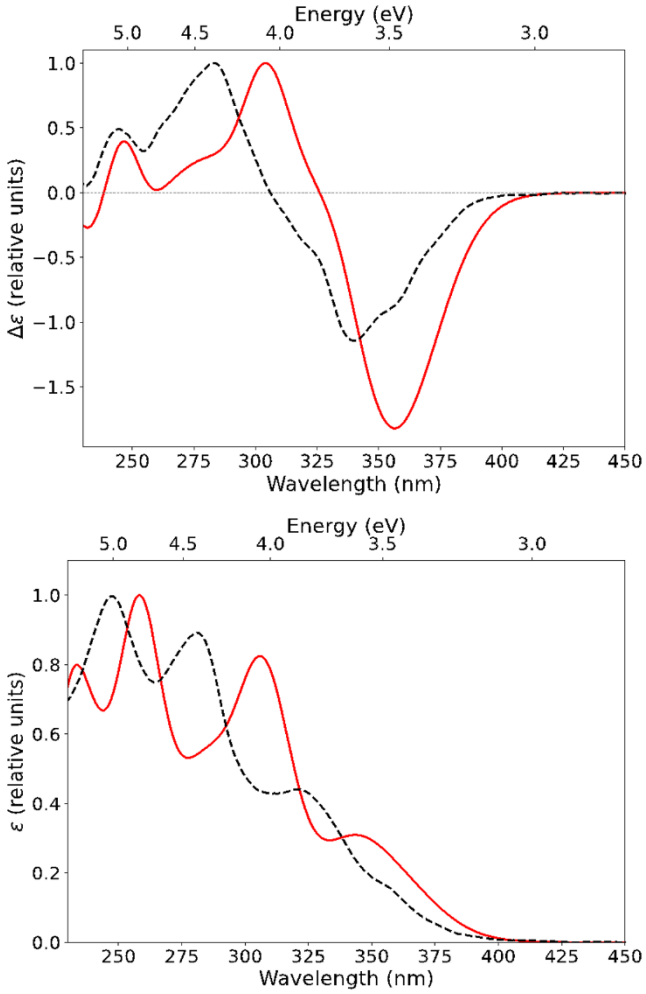

Figure 6. Comparison of the TDA TDDFT simulated (red line) and experimental (black dashed line) CD (top) and UV-Vis (bottom) spectra of **6*M*** in relative units. No spectral shift has been applied. The gaussian broadening of the simulated spectra was performed with a σ value of 0.13 eV.

The absorption and CD spectra of the **6*M*** ligand have been reproduced by time-dependent DFT (TD-DFT) calculations (Figure 6) in a satisfactory manner. The first transition simulated at 380 nm has a weak contribution in both spectra (see Table S3) even if it mainly corresponds to the HOMO ⟶ LUMO transition.

According to natural transition orbital (NTO) analysis, this transition as well as the following ones (E < 4.5 eV) are predominantly assigned to π ⟶ π* transitions localized in the helicene part of the **6*M*** ligand (see NTOs # 1–9, Figure S20). Those transitions lead to the two main bands simulated around 305 and 355 nm in both spectra. At higher energy, the π orbitals contribution of the bpp part of **6*M*** becomes apparent as illustrated by the NTOs of the 21st transition (Figure S19), which is responsible, among others, of the UV-Vis band at 260 nm. In addition to the calculation of the vertical absorption energies, the optimized structure of the first singlet excited state (S_1) and the first three triplet states (T_1, T_2 and T_3) were calculated and included in the Jablonski diagram depicted in Figure 7. The discussed results were established using the length-gauge formalism but comparison with the velocity-gauge adopted-form is available in the ESI (Table S3 and Figure S20).

TD-DFT calculations were then performed on a closed shell form of the complexes where the trivalent lanthanide center was replaced by yttrium(III) (see computational details). NTOs analysis suggests that the first transitions in the whole complex are still centered on the **6*M*** ligand (Figure S21). Contributions from transitions localized on tta$^-$ ligands appear in the range 3.8 – 3.9 eV, like for instance the intense 17th transition. Only few transitions were calculated in this range for the **6*M*** ligand. That explains the evolution of the spectra of the complex in comparison with the **6*M*** based-one (Figure S22), i.e. the red-shift and the higher intensity of the UV-Vis band near 320 nm, and the flattening of the last CD band. Otherwise, the observed CD band around 250 nm is less well reproduced than for the **6*M*** ligand. Its simulated maxima (at 270 nm) are red-shifted, contrary to the general blue-shift of these TD-DFT spectra compared to the experiments. However, this is probably explained by the number of transitions that we were able to calculate, which leads to a potentially inaccurate representation of this band.

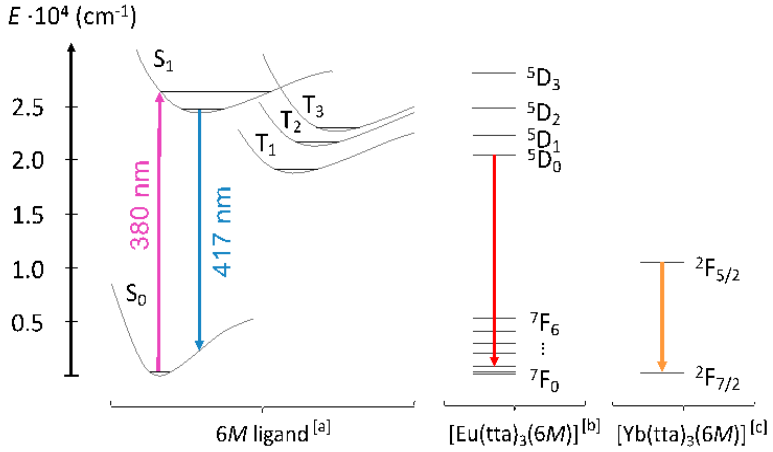

Figure 7. Jablonski diagram depicted with [a] TDA TDDFT, [b] CAS(6,7)SCF and [c] CAS(13,7)SCF calculations.

State average complete active space self-consistent field (SA-CASSCF) method-based calculations allow us to describe the electronic structure and to simulate chiroptical properties of europium(III) and ytterbium(III) complexes (see computational details) as already established in previous works.[50,54] In order to gain insight into the driven luminescence mechanism of both complexes, the Jablonski diagram was completed (Figure 7) by energetic splitting obtained from the SA-CASSCF calculations (Tables S4 and S5). The ^5D_J spectroscopic level of [Eu(tta)$_3$(**6*M***)] are calculated too high in energy. Notably, the emissive $^5D_0$ level is calculated at approx. 3000 cm^{-1} higher than usually expected according to the literature.[55] The luminescence of lanthanide complexes can be explained by the so-called antenna effect.[56] Hence, by assuming the $^5D_0$ level of the [Eu(tta)$_3$(**6*M***)] complex slightly lower in energy (typically near 17 400 cm^{-1}), the energy transfer most likely occurs from the T_1 state of the **6*M*** ligand (while tta$^-$ cannot be discarded) in order to sensitize the Eu(III) ion. This sensitization

pathway, the most commonly accepted,[57] is supported by spin-orbit coupling (SOC) calculations concerning the **6*M*** ligand. Indeed, the most favoured intersystem crossing (ISC) from the S_1 state is with the T_1 state, regardless that the S_1 state of the **6*M*** ligand has time to relax or not after being reached (Table S6). Therefore, even if the tta^- ligands certainly play a role in the Eu(III) sensitization with respect to the literature,[58] the **6*M*** ligand appears to be correctly designed to sensitize also the Eu(III) center.

For the [Yb(tta)$_3$(**6*M***)] complex, the energetic gap between the T_1 state of **6*M*** and its $^2F_{5/2}$ emissive level is too high (about 9 000 cm^{-1}) to enable an efficient energy transfer. Therefore, the sensitization of the Yb(III) ion certainly comes from the tta^- ligands, as already reported in the literature,[59,60] with an indeterminate mechanism.

Dealing then with the lanthanide centered luminescence, the CPL spectrum of the Eu(III) complex was theoretically reproduced (Figure 8). The shape of the band induced by the transitions $^7F_1 \longleftarrow {}^5D_0$ is satisfactory reproduced. For the other bands, a comparison between the theoretical and the experimental CPL spectrum is harder to establish. Furthermore, one notices an important blue-shift for the simulated spectrum due to the missed placement of the $^5D_0$ spectroscopic level previously mentioned. Works along this line are envisaged in a close future to tentatively improve energies of the excited states. Thus, at this stage, the bands calculated around 570 nm certainly correspond to the $^7F_4 \longleftarrow {}^5D_0$ transitions, while, the $^7F_5 \longleftarrow {}^5D_0$ transitions, just like the $^7F_3 \longleftarrow {}^5D_0$ transitions, are calculated with low rotatory strength (Table S7, ESI). These are in accordance with what is predicted by the selection rules for the f–f transitions, in so far as they are respected. Indeed, electric dipole transitions are allowed only for values of ΔJ equal to 2, 4 or 6 as $J' = 0$ for the emissive level. The strict forbidden character of the $^7F_0 \longleftarrow {}^5D_0$ transition with $J = 0$ and $J' = 0$ ($R = 3.41 \cdot 10^{-47}$ esu^2 cm^2) as well as the magnetic dipole character of the $^7F_1 \longleftarrow {}^5D_0$ transition ($f_{MD} \geq 10^3 f_{ED}$, see Table S7) are correctly computed.

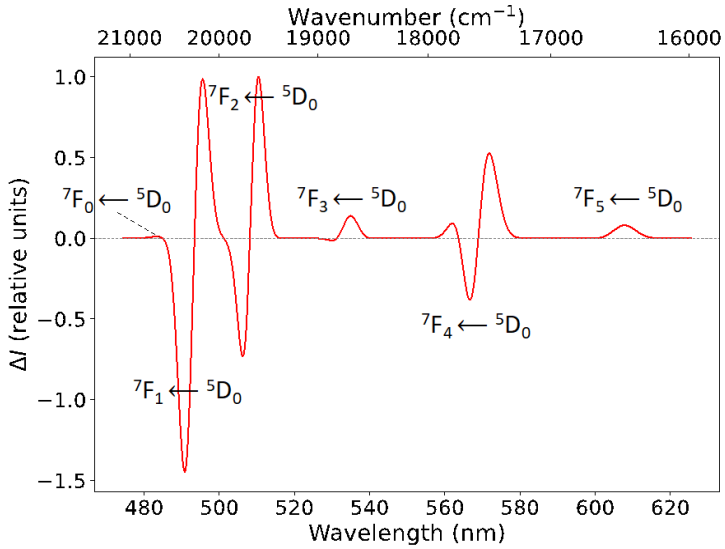

Figure 8. Calculated CPL spectrum of [Eu(tta)$_3$(**6*M***)] complex in relative units. The Gaussian broadening was performed with a σ value of 10 meV. No spectral shift has been applied.

Conclusions

In conclusion, the first enantiopure versions of tridentate bpp-helicene ligands have been prepared and characterized through their structural and chiroptical properties. DFT and TD-DFT could reproduce both absorption and CD spectra of **6*M***, highlighting the contribution of helicene and bpp in the main transitions. These ligands allowed the preparation of emissive Eu(III) and Yb(III) complexes in the visible

and NIR regions, respectively, with the former also showing weak circularly polarized emission. The tta^- ligands completing the coordination sphere of the Ln centers are already known to be able to sensitize the luminescence of lanthanide centers. Nevertheless, according to TD-DFT and CASSCF calculations, the bpp-helicene ligands can also efficiently sensitize the luminescence of Eu(III) center through energy transfer from the first triplet state of the ligand, while the sensitization of Yb(III) should arise from other types of mechanisms. The relatively low values of $\pm 3 \cdot 10^{-3}$ for the CPL dissymmetry factor g_{lum} of the Eu(III) complex, corresponding to the $^7F_1 \longleftarrow {}^5D_0$ transition, are very likely due to the remote location of the chiral space provided by the helicene unit with respect to the coordination sphere of the metal ion. These results open the way towards the preparation of chiral bpp-helicene lanthanide complexes provided with magnetochiral properties. The variation of the positioning of the helicene unit on the bpp platform is of prime importance, in order to promote a stronger polarization of the emission. These strategies are under current investigation in our groups.

Experimental Section

Materials and Methods. The precursors $[Eu(tta)_3(H_2O)_2]$, $[Yb(tta)_3(H_2O)_2]$[60] and 2-bromo[6]helicene[61] were prepared as previously reported in the literature. All other materials and solvents were commercially available and used without further purification. Nuclear magnetic resonance spectra were recorded on a Bruker Avance DRX 300 spectrometer (operating at 300 MHz for ^1H and 75 MHz for ^{13}C). Chemical shifts are expressed in parts per million (ppm) downfield from external TMS. MALDI-TOF MS spectra were recorded on Bruker Biflex-IIITM apparatus, equipped with a 337 nm N_2 laser. Elemental analyses were recorded using Flash 2000 Fisher Scientific Thermo Electron analyser. UV-Vis absorption spectra were recorded using a Shimadzu UV 1800 spectrometer in 10^{-5} M CH_2Cl_2 solutions. Excitation and emission spectra were recorded using a RF-6000 spectrometer in 10^{-6} M CH_2Cl_2 solutions. Absolute quantum yields were determined by using an integrating sphere. CD spectra were recorded on a JASCO J-1500 spectrometer at 20°C. CPL measurements were carried out with a home-made spectrofluoropolarimeter,[62] mounting a Hamamatsu R-376 for visible measurements and a Hamamatsu R-316 for NIR ones.[49] The samples concentration was around $1 \cdot 10^{-5}$ M. A 365 nm LED was used as the excitation source, employing a 90° excitation geometry. Luminescence dissymmetry factors (g_{lum}) were calculated as $2(I_L-I_R)/(I_L+I_R)$, where I_L and I_R are left and right circularly polarized components of the emission. The spectra are the average of eight accumulations each.

Synthesis of 1-bpp[6]helicene. In a Schlenk tube under inert atmosphere, pyrazole (0.91 mmol, 62 mg) was dissolved in diethylene glycol dimethyl ether (6 mL). Sodium hydride (60 %w, 0.91 mmol, 37 mg) was slowly added and the mixture was stirred for 2h at room temperature. Dichloropyridine-[6]helicene (0.32 mmol, 150 mg) was then added and the mixture was refluxed for 5 days. After evaporation of the solvent under vacuum, 15 mL of water was added to precipitate the product. The white powder was dried under vacuum (135 mg, 0.25 mmol, 78% yield). After separation of the two enantiomers by semi-preparative chiral HPLC, single crystals of **6*M*** and **6*P*** were obtained by slow evaporation of an acetone solution. ^1H NMR (300 MHz, $CDCl_3$) : δ 8.52 (d, *J* = 2.5 Hz, 2H, H1-H4), 8.15 (d, *J* = 8.6 Hz, 1H), 8.16 (m, 1H), 8.04 – 7.93 (m, 8H), 7.87 (d, *J* = 1.1 Hz, 2H), 7.65 (ddd, J = 8.4, 7.8, 1.7 Hz, 2H, H3-H6), 7.31 (s, 2H, H7-H8), 7.20 (ddd, *J* = 8.1, 6.9, 1.2 Hz, 1H), 6.72 (ddd, *J* = 8.3, 6.9, 1.3 Hz, 1H), 6.51 (dd, *J* = 2.5, 1.7 Hz, 2H, H2-H5). ^{13}C NMR (75 MHz, $CDCl_3$) : δ 154.3, 150.3, 142.1, 134.3, 133.2, 132.4, 132.4, 131.8, 131.7, 130.2, 129.6, 128.7, 128.7, 128.2, 127.9, 127.7, 127.7, 127.5, 127.2, 127.0, 125.8, 124.8, 124.1, 107.9, 107.6. MALDI: 537.

General procedure for the synthesis of $[Ln(tta)_3(6M)]$ and $[Ln(tta)_3(6P)]$. The ligand enantiomer **6*M*** or **6*P*** (0.029 mmol, 15.5 mg) was dissolved in acetone (4 mL) and placed under argon atmosphere. A solution of $[Ln(tta)_3(H_2O)_2]$ (0.029 mmol, 25 mg for Ln = Eu and 26 mg for Ln = Yb) in acetone (1 mL) was added and the mixture was stirred at 50°C for 4 hours. The solvent was evaporated under vacuum and the residue was dissolved in a minimum of dichloromethane. Precipitation by addition of *n*-hexane

gave the desired product as a yellow powder. Yields: between 56 and 62%. MALDI: 1130, $[Eu(tta)_2(\mathbf{6M})]^+$ and $[Eu(tta)_2(\mathbf{6P})]^+$; 1153, $[Yb(tta)_2(\mathbf{6M})]^+$ and $[Yb(tta)_2(\mathbf{6P})]^+$. Anal. calcd. for $C_{61}H_{35}N_5O_6S_3F_9Eu$: C, 54.15, H, 2.61, N, 5.18%. Found: C, 54.00, H, 2.48, N, 4.98%. Anal. calcd. for $C_{61}H_{35}N_5O_6S_3F_9Yb$: C, 53.32, H, 2.57, N, 5.10%. Found: C, 53.05, H, 2.39, N, 4.85%.

Structural Characterization. Single crystals of the compounds were mounted on glass fiber loops using a viscous hydrocarbon oil to coat the crystal and then transferred directly to the cold nitrogen stream for data collection. Data collections were performed at 150 K on an Agilent Supernova with CuKα (λ = 1.54184 Å). The structures were solved by direct methods with the SIR97 program and refined against all F^2 values with the SHELXL-97 program[63] using the WinGX graphical user interface.[64] All non-hydrogen atoms were refined anisotropically except as noted. Hydrogen atoms were placed in calculated positions and refined isotropically with a riding model. CCDC 2101184 (**6*M***) and CCDC 2101185 (**6*P***) contain the supplementary crystallographic data for this paper. This data can be obtained free of charge from The Cambridge Crystallographic Data Centre via www.ccdc.cam.ac.uk/data_request/cif.

Computational details. The Kohn-Sham density functional theory (DFT) and the time-dependent DFT (TDDFT) calculations were carried out with the 2019's release of the Amsterdam Density Functional (ADF)[65,66] program. All calculations utilized the zeroth-order regular approximation (ZORA)[67,68] along with the hybrid functional PBE0[69,70] with 25% of exact exchange and the atomic basis set corresponding to the triple-ζ polarized Slater-type orbital (STO) all-electron basis set with one set of polarization functions for all atoms (TZP).[71] No symmetry has been imposed for all computations. Solvent effects of the dichloromethane (DCM) were considered by using the Conductor-Like Screening Model (COSMO)[72] with the dielectric constant of 8.9. From the X-Ray characterized structure of **6*M***, two different conformers have been optimized and the more stable one was retained for the following calculations. Frequencies calculations were performed to ensure that no imaginary frequencies were present.[73] TD-DFT linear response calculations of the 100 lowest singlet excitation energies have been computed using the Tamm-Dancoff approximation (TDA).[74] The oscillator and the rotatory strengths were analytically calculated in their length and velocity gauge forms.[75] The nature of the transitions was analyzed with the help of the Natural Transition Orbitals (NTOs),[76] visualized with the graphical user interface of ADF. The optimized structures with their associated energy of the lowest excited states were obtained using TDA TD-DFT. The spin-orbit coupling (SOC) between the first five excited singlet and triplet states have been computed perturbatively[77] at the geometry of the ground state (S_0) and of the first singlet excited state (S_1). Next, the $[Eu(tta)_3(\mathbf{6M})]$ and $[Yb(tta)_3(\mathbf{6M})]$ complexes have been studied. One structural arrangement of the complex was firstly optimized in a closed shell system where the metallic center was replaced by Yttrium(III). Based on this geometry, TDA TD-DFT calculation covering up to 100 singlet excited states was performed. The Yttrium(III) ionic center was also replaced by Europium(III) and Ytterbium(III) in order to obtain a ground state structure of the complexes with a spin multiplicity of 7 and 2, respectively. For these two DFT optimizations, the COSMO model of DCM was not used and the resulting structures were employed to run multi-configurational calculations in gas phase. The wave function-based calculations have been done through the state average (SA) complete active space (CAS) self-consistent field (SCF) approach with the *OpenMolcas* quantum-chemistry package (version 19.11).[78] The all-electron atomic natural orbital relativistic contracted (ANO-RCC) basis sets from the Molcas library were used.[79] The following contractions were employed for Eu and Yb [25s22p15d11f4g2h/8s7p4d3f2g1h], for O and N [14s9p4d3f2g/4s3p2d1f], for C and F [14s9p4d3f2g/3s2p], and for H [8s4p3d1f/2s]. In addition to these basis sets, the second-order Douglas-Kroll-Hess scalar relativistic Hamiltonian[80] was used to consider the scalar relativistic (SR) effects. The CAS was filled by the seven 4f orbitals of the lanthanide trivalent ionic center and by the corresponding 4f populated number of electrons (i.e. CAS(6,7) and CAS(13,7) for Eu^{III} and Yb^{III} respectively). To describe the $[Eu(tta)_3(\mathbf{6M})]$ complex, all septet spin sates (7 roots), 105 quintets, 141 triplets and 26 singlets were calculated while for the $[Yb(tta)_3(\mathbf{6M})]$ complex all roots

were computed (7 septets). SOC was then added within the restricted active space state interaction (RASSI) method by mixing the SA-CASSCF wave functions.[81] For all these wave function-based calculations, Cholesky decomposition of the bi-electronic integrals was employed,[82] to save disk space and to speed up the calculations, and SOC integrals were calculated using the atomic mean-field integrals (AMFI) approximation.[83] The TD-DFT spectra were scaled by Gaussian function from oscillator strength *f* or rotatory strength *R* with a σ value of 0.13 eV. No spectral shift has been applied. The CPL spectrum was obtained by exploiting SA-CASSCF results as detailed in our previous work.[54]

Acknowledgements

This work was supported in France by the CNRS, the University of Angers and the RFI LUMOMAT (ASCO MMM Project). The French National Research Agency (ANR) is acknowledged for financial support through SMMCPL (ANR-19-CE29-0012-02) and SECRETS (ANR PRC 20-CE06-0023-01) projects. M.G. and B.L.G. thank the French GENCI/IDRIS-CINES centers for high performance computing resources. F.Z. gratefully acknowledges financial support from University of Pisa (PRA 2020_21).

Keywords

Bis(pyrazolyl)-pyridine ligands · Circular Dichroism · Circularly polarized luminescence · Helicenes · Lanthanide complexes

Notes and references

[1] F. Pop, N. Zigon, N. Avarvari, *Chem. Rev.* **2019**, *119*, 8435–8478.
[2] M. Gingras, *Chem. Soc. Rev.* **2013**, *42*, 1051–1095.
[3] K. Dhbaibi, L. Favereau, J. Crassous, *Chem. Rev.* **2019**, *119*, 8846–8853.
[4] J. Míšek, F. Teplý, I. G. Stará, M. Tichý, D. Šaman, I. Císařová, P. Vojtíšek, I. Starý, *Angew. Chem. Int. Ed.* **2008**, *47*, 3188–3191.
[5] N. Saleh, C. Shen, J. Crassous, *Chem. Sci.* **2014**, *5*, 3680–3694.
[6] C. Shen, G. Loas, M. Srebro-Hooper, N. Vanthuyne, L. Toupet, O. Cador, F. Paul, J. T. López Navarrete, F. J. Ramírez, B. Nieto-Ortega, J. Casado, J. Autschbach, M. Vallet, J. Crassous, *Angew. Chem. Int. Ed.* **2016**, *28*, 8062–8066.
[7] H. Isla, M. Srebro-Hooper, M. Jean, N. Vanthuyne, T. Roisnel, J. L. Lunkley, G. Muller, J. A. Gareth Williams, J. Autschbach, J. Crassous, *Chem. Commun.* **2016**, *52*, 5932–5935.
[8] N. Saleh, B. Moore, M. Srebro, N. Vanthuyne, L. Toupet, J. A. Gareth Williams, C. Roussel, K. K. Deol, G. Muller, J. Autschbach, J. Crassous, *Chem. Eur. J.* **2015**, *21*, 1673–1681.
[9] T. Biet, T. Cauchy, Q. Sun, J. Ding, A. Hauser, P. Oulevey, T. Bürgi, D. Jacquemin, N. Vanthuyne, J. Crassous, N. Avarvari, *Chem. Commun.* **2017**, *53*, 9210–9213.
[10] F. Pointillart, J.-K. Ou-Yang, G. Fernandez Garcia, V. Montigaud, J. Flores Gonzales, R. Marchal, L. Favereau, F. Totti, J. Crassous, O. Cador, L. Ouahab, B. Le Guennic, *Inorg. Chem.* **2019**, *58*, 52–56.
[11] J.-K. Ou-Yang, N. Saleh, G. Fernandez Garcia, L. Norel, F. Pointillart, T. Guizouarn, O. Cador, F. Totti, L. Ouahab, J. Crassous, B. Le Guennic, *Chem. Commun.* **2016**, *52*, 14474–14477.
[12] M. Atzori, K. Dhbaibi, H. Douib, M. Grasser, V. Dorcet, I. Breslavetz, K. Paillot, O. Cador, G. L. J. A. Rikken, B. Le Guennic, J. Crassous, F. Pointillart, C. Train, *J. Am. Chem. Soc.* **2021**, *143*, 2671–2675.
[13] T. Biet, A. Fihey, T. Cauchy, N. Vanthuyne, C. Roussel, J. Crassous, N. Avarvari, *Chem. Eur. J.* **2013**, *19*, 13160–13167.
[14] T. Biet, K. Martin, J. Hankache, N. Hellou, A. Hauser, T. Bürgi, N. Vanthuyne, T. Aharon, M. Caricato, J. Crassous, N. Avarvari, *Chem. Eur. J.* **2017**, *23*, 437–446.
[15] M. Savchuk, S. Vertueux, T. Cauchy, M. Loumaigne, F. Zinna, L. Di Bari, N. Zigon, N. Avarvari, *Dalton Trans.* **2021**, *50*, 10533–10539.
[16] A. Abhervé, K. Martin, A. Hauser, N. Avarvari, *Eur. J. Inorg. Chem.* **2019**, 4807–4814.
[17] M. A. Halcrow, *Coord. Chem. Rev.* **2005**, *249*, 2880–2908.
[18] M. Attwood, S. S. Turner, *Coord. Chem. Rev.* **2017**, *353*, 247–277.
[19] A. A. Watson, D. A. House, P. J. Steel, *J. Org. Chem.* **1991**, *56*, 4072–4074.

[20] R. Kowalczyk, J. Skarzewski, *Tetrahedron* **2005**, *61*, 623–628.
[21] D. L. Christenson, C. J. Tokar, W. B. Tolman, *Organometallics* **1995**, *14*, 2148–2150.
[22] W.-H. Fung, W.-C. Cheng, W.-Y. Yu, C.-M. Che, T. C. W. Mak, *J. Chem. Soc., Chem. Commun.* **1995**, 2007–2008.
[23] M. A. Halcrow, *New J. Chem.* **2014**, *38*, 1868–1882.
[24] J. M. Stanley, X. Zhu, X. Yang, B. J. Holliday, *Inorg. Chem.* **2010**, *49*, 2035–2037.
[25] M. Starck, R. Ziessel, *Dalton Trans.* **2012**, *41*, 13298–13307.
[26] M. Feng, S. Speed, F. Pointillart, B. Lefeuvre, B. Le Guennic, S. Golhen, O. Cador, L. Ouahab, *Eur. J. Inorg. Chem.* **2016**, 2039–2050.
[27] R. S. Dickens, J. A. K. Howard, C. L. Maupin, J. M. Moloney, D. Parker, R. D. Peacock, J. P. Riehl, G. Siligardi, *New J. Chem.* **1998**, *22*, 891–899.
[28] D. G. Smith, R. Pal, D. Parker, *Chem. Eur. J.* **2012**, *18*, 11604–11613.
[29] R. S. Dickins, J. A. K. Howard, C. L. Maupin, J. M. Moloney, D. Parker, J. P. Riehl, G. Siligardi, J. A. G. Williams, *Chem. Eur. J.* **1999**, *5*, 1095–1105.
[30] J. K. Molloy, O. Kotova, R. D. Peacock, T. Gunnlaugsson, *Org. Biomol. Chem.* **2012**, *10*, 314–322.
[31] D. G. Smith, B. K. McMahon, R. Pal, D. Parker, *Chem. Commun.* **2012**, *48*, 8520–8522.
[32] L. Dai, W.-S. Lo, I. D. Coates, R. Pal, G.-L. Law, *Inorg. Chem.* **2016**, *55*, 9065–9070.
[33] J. L. Lunkley, D. Shirotani, K. Yamanari, S. Kaizaki, G. Muller, *Inorg. Chem.* **2011**, *50*, 12724–12732.
[34] Z. Li, H. Minami, K. Nakamura, N. Kobayashi, *ChemPhysChem* **2021**, *22*, 2511–2516.
[35] T. Harada, Y. Nakano, M. Fujiki, M. Naito, T. Kawai, Y. Hasegawa, *Inorg. Chem.* **2009**, *48*, 11242–11250.
[36] T. Harada, H. Tsumatori, K. Nishiyama, J. Yuasa, Y. Hasegawa, T. Kawai, *Inorg. Chem.* **2012**, *51*, 6476–6485.
[37] F. Zinna, C. Resta, S. Abbate, E. Castiglioni, G. Longhi, P. Mineo, L. Di Bari, *Chem. Commun.* **2015**, *51*, 11903–11906.
[38] J. P. Leonard, P. Jensen, T. McCabe, J. E. O'Brien, R. D. Peacock, P. E. Kruger, T. Gunnlaugsson, *J. Am. Chem. Soc.* **2007**, *129*, 10986–10987.
[39] M. Starck, L. E. MacKenzie, A. S. Batsanov, D. Parker, R. Pal, *Chem. Commun.* **2019**, *55*, 14115–14118.
[40] D. E. Barry, J. A. Kitchen, L. Mercs, R. D. Peacock, M. Albrecht, T. Gunnlaugsson, *Dalton Trans.* **2019**, *48*, 11317–11325.
[41] G. Bozoklu, C. Gateau, D. Imbert, J. Pécaut, K. Robeyns, Y. Filinchuk, F. Memon, G. Muller, M. Mazzanti, *J. Am. Chem. Soc.* **2012**, *134*, 8372–8375.
[42] L. Arrico, C. Benetti, L. Di Bari, *ChemPhotoChem* **2021**, *5*, 815–821.
[43] E. Kreidt, L. Arrico, F. Zinna, L. Di Bari, M. Seitz, *Chem. Eur. J.* **2018**, *24*, 13556–13564.
[44] C. Dee, F. Zinna, E. Kreidt, L. Arrico, A. Rodríguez-Rodríguez, C. Platas-Iglesias, L. Di Bari, M. Seitz, *J. Rare Earths* **2020**, *38*, 564–570.
[45] S. Di Pietro, L. Di Bari, *Inorg. Chem.* **2012**, *51*, 12007–12014.
[46] F. Zinna, L. Di Bari, *Chirality* **2014**, *27*, 1-13.
[47] J. Yuasa, T. Ohno, K. Miyata, H. Tsumatori, Y. Hasegawa, T. Kawai, *J. Am. Chem. Soc.* **2011**, *133*, 9892–9902.
[48] M. Górecki, L. Carpita, L. Arrico, F. Zinna, L. Di Bari, *Dalton Trans.* **2018**, *47*, 7166–7177.
[49] F. Zinna, L. Arrico, L. Di Bari, *Chem. Commun.* **2019**, *55*, 6607–6609.
[50] F. Gendron, S. Di Pietro, L. Abad Galan, F. Riobé, V. Placide, L. Guy, F. Zinna, L. Di Bari, A. Bensalah-Ledoux, Y. Guyoy, G. Pilet, F. Pointillart, B. Baguenard, S. Guy, O. Cador, O. Maury, B. Le Guennic, *Inorg. Chem. Front.* **2021**, *8*, 914–926.
[51] B. Lefeuvre, C. A. Mattei, J. Flores Gonzalez, F. Gendron, V. Dorcet, F. Riobé, C. Lalli, B. Le Guennic, O. Cador, O. Maury, S. Guy, A. Bensalah-Ledoux, B. Baguenard, F. Pointillart, *Chem. Eur. J.* **2021**, *27*, 7362–7366.
[52] C. L. Maupin, D. Parker, J. A. G. Williams, J. P. Riehl, *J. Am. Chem. Soc.* **1998,** *120,* 10563–10564.
[53] C. L. Maupin, R. S. Dickins, L. G. Govenlock, C. E. Mathieu, D. Parker, J. A. G. Williams, J. P. Riehl, *J. Phys. Chem. A* **2000**, *104*, 6709–6717.
[54] F. Gendron, B. Moore II, O. Cador, F. Pointillart, J. Autschbach, B. Le Guennic, *J. Chem. Theory Comput.* **2019**, *15*, 4140–4155.
[55] G. H. Dieke, H. M. Crosswhite, *Appl. Opt.* **1963**, *2*, 675–686.
[56] S. V. Eliseeva, J.-C. G. Bünzli, *Chem. Soc. Rev.* **2010**, *39*, 189–227.
[57] A. D'Aléo, F. Pointillart, L. Ouahab, C. Andraud, O. Maury, *Coord. Chem. Rev.* **2012**, *256*, 1604–1620.
[58] C. Freund, W. Porzio, U. Giovanella, F. Vignali, M. Pasini, S. Destri, A. Mech, S. Di Pietro, L. Di Bari, P. Mineo, *Inorg. Chem.* **2011**, *50*, 5417–6429.
[59] B. Li, H. Li, P. Chen, W. Sun, C. Wang, T. Gao, P. Yan, *Phys. Chem. Chem. Phys.* **2015**, *17*, 30510–30517.
[60] A. I. Voloshin, N. M. Shavaleev, V. P. Kazakov, *J. Lumin.* **2000**, *91*, 49–58.

[61] M. Jakubec, T. Beránek, P. Jakubík, J. Sýkora, J. Žádný, V. Církva, J. Storch, *J. Org. Chem.* **2018**, *83*, 3607–3616.

[62] F. Zinna, T. Bruhn, C. A. Guido, J. Ahrens, M. Bröring, L. Di Bari, G. Pescitelli, *Chem. Eur. J.* **2016**, *22*, 16089–16098.

[63] G. M. Sheldrick, *Programs for the Refinement of Crystal Structures;* University of Göttingen: Göttingen, Germany, **1996**.

[64] L. J. Farrugia, *J. Appl. Crystallogr.* **1999**, *32*, 837–838.

[65] G. te Velde, F. M. Bickelhaupt, E. J. Baerends, S. J. A. van Gisbergen, C. Fonseca Guerra, J. G. Snijders, T. Ziegler, *J. Comput. Chem.* **2001**, *22*, 931–967.

[66] E. J. Baerends, T. Ziegler, A. J. Atkins, J. Autschbach, O. Baseggio, D. Bashford, A. Bérces, F. M. Bickelhaupt, C. Bo, P.M. Boerrigter, L. Cavallo, C. Daul, D. P. Chong, D. V. Chulhai, L. Deng, R. M. Dickson, J. M. Dieterich, D. E. Ellis, M. van Faassen, L. Fan, T. H. Fischer, A. Förster, C. Fonseca Guerra, M. Franchini, A. Ghysels, A. Giammona, S. J. A. van Gisbergen, A. Goez, A. W. Götz, J. A. Groeneveld, O. V. Gritsenko, M. Grüning, S. Gusarov, F. E. Harris, P. van den Hoek, Z. Hu, C. R. Jacob, H. Jacobsen, L. Jensen, L. Joubert, J. W. Kaminski, G. van Kessel, C. König, F. Kootstra, A. Kovalenko, M. V. Krykunov,; E.van Lenthe, D. A. McCormack, A. Michalak, M. Mitoraj, S. M. Morton, J. Neugebauer, V. P. Nicu, L. Noodleman, V. P. Osinga, S. Patchkovskii, M. Pavanello, C. A. Peeples, P. H. T. Philipsen, D. Post, C. C. Pye, H. Ramanantoanina, P. Ramos, W. Ravenek, J. I. Rodríguez, P. Ros, R. Rüger, P. R. T. Schipper, D. Schlüns, H. van Schoot, G. Schreckenbach, J. S. Seldenthuis, M. Seth, J. G. Snijders, M. Solà, M. Stener, M. Swart, D. Swerhone, V. Tognetti, G. te Velde, P. Vernooijs, L. Versluis, L. Visscher, O. Visser, F. Wang, T. A. Wesolowski, E. M. vanWezenbeek, G. Wiesenekker, S. K. Wolff, T. K. Woo, A. L. Yakovlev, ADF 2019, SCM, Theoretical Chemistry, Vrije Universiteit, Amsterdam, The Netherlands, http://www.scm.com, **2019**.

[67] E. van Lenthe, E. J. Baerends, J. G. Snijders, *J. Chem. Phys.* **1993**, *99*, 4597–4610.

[68] E. van Lenthe, A. E. Ehlers, E. J. Baerends, *J. Chem. Phys.* **1999**, *110*, 8943–8953.

[69] M. Ernzerhof, G. E. Scuseria, *J. Chem. Phys.* **1999**, *110*, 5029–5036.

[70] C. Adamo, V. Barone, *J. Chem. Phys.* **1999**, *110*, 6158–6170.

[71] E. van Lenthe, E. J. Baerends, *J. Comput. Chem.* **2003**, *24*, 1142–1156.

[72] C. C. Pye, T. Ziegler, *Theor. Chem. Acc.* **1999**, *101*, 396–408.

[73] L. Fan, T. Ziegler, *J. Chem. Phys.* **1992**, *96*, 9005.

[74] S. Hirata, M. Head-Gordon, *Chem. Phys. Lett.* **1999**, *314*, 291–299.

[75] J. Autschbach, S. J. A. van Gisbergen, T. Ziegler, *J. Chem. Phys.* **2002**, *116*, 6930–6940.

[76] R. L. Martin, *J. Chem. Phys.* **2003**, *118*, 4775–4777.

[77] F. Wang, T. Ziegler, *J. Chem. Phys.* **2005**, *123*, 154102.

[78] I. F. Galván, M. Vacher, A. Alavi, C. Angeli, F. Aquilante, J. Autschbach, J. J. Bao, S. I. Bokarev, N. A. Bogdanov, R. K. Carlson, L. F. Chibotaru, J. Creutzberg, N. Dattani, M. l G. Delcey, S. S. Dong, A. Dreuw, L. Freitag, L. Manuel Frutos, L. Gagliardi, F. Gendron, A. Giussani, L. González, G. Grell, M. Guo, C. E. Hoyer, M. Johansson, S. Keller, S. Knecht, G. Kovacevic, E. K. llman, G. Li Manni, M. Lundberg, Y. Ma, S. Mai, J. P. Malhado, P. Malmqvist, P. Marquetand, S. A. Mewes, J. Norell, M. Olivucci, M. Oppel, Q. M. Phung, K. Pierloot, F. Plasser, M. Reiher, A. M. Sand, I. Schapiro, P. Sharma, C. J. Stein, L. K. Sørensen, D. G. Truhlar, M. Ugandi, L. Ungur, A. Valentini, S. Vancoillie, V. Veryazov, O. Weser, T. A. Wesołowski, P.-O. Widmark, S. Wouters, A. Zech, J. Patrick Zobel, R. Lindh, *J. Chem. Theory Comput.* **2019**, *15*, 5925–5964.

[79] a) P.-O. Widmark, P.-Å. Malmqvist, B. O. Roos, *Theor. Chim. Acta* **1990**, *77*, 291–306; b) B. O. Roos, R. Lindh, P.-Å. Malmqvist, V. Veryazov, P.-O. Widmark, *J. Phys. Chem. A* **2004**, *108*, 2851–2858; c) B. O. Roos, R. Lindh, P.-Å. Malmqvist, V. Veryazov, P.-O. Widmark, *J. Phys. Chem. A* **2005**, *109*, 6575–6579.

[80] a) M. Douglas, N. M. Kroll, *Ann. Phys.* **1974**, *82*, 89–155; b) B. A. Hess, *Phys. Rev. A* **1985**, *32*, 756–763; c) B. A. Hess, *Phys. Rev. A* **1986**, *33*, 3742–3748; d) A. Wolf, M. Reiher, B. A. Hess, *J. Chem. Phys.* **2002**, *117*, 9215–9226.

[81] P.-A. Malmqvist, B. O. Roos, B. Schimmelpfennig, *Chem. Phys. Lett.* **2002**, *357*, 230–240.

[82] F. Aquilante, R. Lindh, T. B. Pedersen, *J. Chem. Phys.* **2007**, *127*, 114107.

[83] B. A. Hess, C. M. Marian, U. Wahlgren, O. A. Gropen, *Chem. Phys. Lett.* **1996**, *251*, 365–371.

10.1002/ejic.202200010

Table of Contents Entry

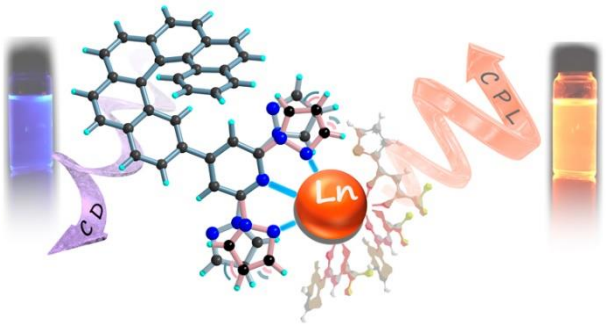

The use of enantiopure bis(pyrazolyl)-pyridine-[6]helicene ligands allowed the preparation of chiral emissive Eu(III) and Yb(III) complexes. Remarkably, the Eu(III) complex shows CPL activity despite of the remote position of the helicene unit with respect to the coordination sphere of the metal ion.